Available online at www.sciencedirect.com
ScienceDirect
International Journal of Mass Spectrometry 260 (2007) 137–145
International Journal of Mass Spectrometry
www.elsevier.com/locate/ijms

Imaging and differentiation of mouse embryo tissues by ToF-SIMS

Ligang Wu [a,b], Xiaochen Lu [b], Kristen S. Kulp [b], Mark G. Knize [b], Elena S.F. Berman [b], Erik J. Nelson [b], James S. Felton [a,b], Kuang Jen J. Wu [b,*]

[a] *Department of Applied Science, University of California-Davis, Davis, CA 95616, United States*
[b] *Chemistry, Materials and Life Sciences Directorate, Lawrence Livermore National Laboratory, Livermore, CA 94551, United States*

Received 1 June 2006; received in revised form 11 September 2006; accepted 11 September 2006
Available online 8 December 2006

Abstract

Time-of-flight secondary ion mass spectrometry (ToF-SIMS) equipped with a gold ion gun was used to image mouse embryo sections and differentiate tissue types (brain, spinal cord, skull, rib, heart and liver). Embryos were paraffin-embedded and then deparaffinized. The robustness and repeatability of the method was determined by analyzing ten tissue slices from three different embryos over a period of several weeks. Using principal component analysis (PCA) to reduce the spectral data generated by ToF-SIMS, histopathologically identified tissue types of the mouse embryos can be differentiated based on the characteristic differences in their mass spectra. These results demonstrate the ability of ToF-SIMS to determine subtle chemical differences even in fixed histological specimens.
Published by Elsevier B.V.

Keywords: ToF-SIMS; Mouse embryo; Paraffin-embedded; Image PCA

1. Introduction

Formalin-fixed paraffin-embedded (FFPE) tumor samples are routinely used for disease diagnosis and are one of the most important and most abundant sources of clinical samples available in medical centers and medical schools. New technologies for analyzing these samples that could be used to improve tissue-based diagnosis, predict response to specific modes of treatment, and aid in prognosis decisions have the potential to greatly improve decisions about therapeutic strategies.

Beyond the conventional histopathological methods, little has been done to develop new methods to analyze FFPE tissues. Jaremko et al. has applied MALDI-ToF MS to the genotyping of low quality DNA obtained from FFPE tissues [1]. However, no studies have been done to investigate the distribution of small molecules in FFPE tissues. We are using bioimaging time-of-flight secondary ion mass spectrometry (ToF-SIMS) to image tissues by their secondary ions in deparaffinized mouse embryo sections. We then differentiate these tissues based on differences in small molecules remaining after paraffin-embedding and fragments of the tissue proteins. These experiments serve as a preliminary study for further investigation of human FFPE samples from tumor and normal tissues.

Time-of-flight secondary ion mass spectrometry (ToF-SIMS) is a surface-sensitive technique that allows the detection and localization of the chemical composition of sample surfaces. The instrument uses a finely focused (∼300 nm), pulsed primary ion beam to desorb and ionize molecular species from a sample surface. The resulting secondary ions are accelerated into a mass spectrometer, where they are analyzed for mass by measuring their time-of-flight from the sample surface to the detector. Displaying the mass spectra that were collected from the sample surface generates chemical images. The resulting ion images contain a mass spectrum in each pixel of the 256 × 256 pixels in an image. These mass spectra are used to create secondary ion images that reflect the composition and distribution of sample surface constituents.

Using ToF-SIMS technology, several groups have been successful in identifying intracellular distributions of specific biological ions such as sodium, potassium, calcium and membrane lipid fragments [2–11]. Quong et al. showed that in human breast cells exposed to the carcinogen PhIP, the target compound was found in detectable amounts within the outer leaflet membrane of the cells [12]. Similarly, analysis of yeast cells that had

* Corresponding author at: Chemistry, Materials and Life Sciences Directorate, Lawrence Livermore National Laboratory, P.O. Box 808, Livermore, CA 94551, United States. Tel.: +1 925 422 1915.
E-mail address: wu17@llnl.gov (K.J.J. Wu).

1387-3806/$ – see front matter. Published by Elsevier B.V.
doi:10.1016/j.ijms.2006.09.029

been exposed to the drug clofazimine demonstrated the presence of the drug within the cells [8].

Very little has been done to apply ToF-SIMS imaging to cancer or tissue-specific problems. Mouse brain tissue slices have been analyzed using gallium, indium, or gold cluster as a source of primary ions [13–15]. Nygren and Borner demonstrated localization of phosphocholine, galactosylceramide, and cholesterol in rat brain slices using a bismuth cluster ion source [16–18]. Imaging cancer cells grown in culture has also been shown [19–21]. These studies illustrate the ability of ToF-SIMS to sensitively analyze and localize small molecules and large molecule fragments in cells and tissues.

A strength of the ToF-SIMS technique arises from the data generated; each ion image provides a highly detailed mass spectral map of the sample being analyzed. However, the spectra of biological samples are extremely complex and difficult to interpret. This complexity is derived from the contribution of secondary ions that are generated from fragmentation of larger molecules within the sample and matrix effects that influence the secondary ion yield depending on the chemical environment of the surface being sampled [22]. Further, because most of a cell's mass is comprised of proteins, which are composed of only 20 fairly homogenously distributed amino acids, there is a lack of unique peaks among different biological samples. In fact, mass spectra obtained from different types of biological materials qualitatively appear very similar. Therefore, data reduction and pattern recognition statistical analysis techniques must be used to differentiate similar biological materials.

Principal component analysis (PCA) is commonly used to identify similarities and differences in ToF-SIMS spectra and classify spectra into groups [19,22–26]. PCA is a standard, unsupervised multivariate statistical technique which reduces a large data matrix to a few manageable variables called principal components (PCs). Principal components represent linear combinations of the original data and capture the greatest variation in the data set. By plotting the resulting 'scores' and 'loading' plots, the relationship between samples and variables can be visualized and easily interpreted. Wagner and Castner have used PCA and singular value decomposition to successfully cluster ToF-SIMS mass spectra generated from samples of single proteins and from samples of alkanethiol self-assembled monolayers, adsorbed onto gold substrates [22,27–29]. Statistical analysis of ToF-SIMS spectra has also been employed to distinguish three species of freeze-dried yeasts based on membrane phospholipids [11] and to discriminate four yeast strains based on composite spectra from samples of yeast cultures [30]. Vegetative Bacillis cells were discriminated from spores based on ToF-SIMS analysis of phospholipid fragments [25]. We have shown that ToF-SIMS imaging and PCA can differentiate whole cells and homogenates of three carcinoma-derived human breast cancer cell lines (MCF-7, T47D and MDA-MB-231) [21].

This study extends the analytical capabilities of ToF-SIMS and PCA by imaging and differentiating histopathologically identified tissues from 16-day-old FFPE mouse embryos. In this study we demonstrate differentiation of six tissue types and show the reproducibility and robustness of the analysis. These experiments provide the foundation for work with human FFPE tissues and suggest new uses for ToF-SIMS for molecular pathology.

2. Experimental

2.1. Animals

Female C57BL/6BAC mice were purchased from the Jackson Laboratory (Bar Harbor, Maine) and bred with male C57BL/6BAC mice to generate the embryos used in this experiment. The animals were maintained on a 12-h dark/light cycle in a temperature and humidity controlled room. The care of the animals was in accord with the Lawrence Livermore National Laboratory (LLNL) Institutional Animal Care and Use Committee (IACUC) committee guidelines. Animals are anesthetized with isoflurane and killed through cervical dislocation. Embryos were harvested using standard techniques [31].

2.2. Mouse embryo tissue slice preparation

Three 16-day-old mouse embryos from three different dams designated with the numbers 1 to 3 were fixed in 4% paraformaldehye for 36 h and embedded in paraffin blocks using standard techniques [32]. Four-micron thick saggital slice sections were cut from each embryo using a Leica RM2165 microtome and were designated as sections 1 through 9. A fourth slice was cut from the third embryo and was designated as section 10. The sections were placed on 1.2 cm × 1.2 cm silicon (Si) wafer substrates and incubated at 40 °C for overnight. The samples were then deparaffinized and dehydrated using xylene and 100% ethanol. The samples were allowed to air dry and were stored in vacuum at 1E−4 Torr for 24 h before ToF-SIMS analysis.

A fourth mouse embryo was prepared as described above for optical imaging. A 4 μm section was cut and stained with hematoxylin and eosin (H&E) using standard immunohistochemical techniques [32]. The sample was placed on a glass slide and evaluated by the pathologist, Dr. Lu. The identified tissues in this sample were used as a reference for the ToF-SIMS analysis.

2.3. ToF-SIMS analysis

ToF-SIMS measurements were conducted on a PHI-TRIFT III instrument (Physical Electronics USA, Chanhassen, MN) equipped with a gold liquid metal ion gun (Au LMIG). The ion gun was operated at 22 kV and in an unbunched mode. Positive ion SIMS analyses were done utilizing Au^+ ions at room temperature, with a pulsed, low-energy electron gun providing charge neutralization. For the tissue differentiation experiment, six tissue types were selected from section number 10: skull, rib, brain, spinal cord, heart and liver. Tissues were identified based on the pathologist's designation of similar tissue regions in the H&E stained section. ToF-SIMS measurements were conducted over a 300 μm × 300 μm area for 5 min; one average mass spectrum was reconstructed for that specific region of the tissue section. Ten measurements were recorded for each tissue type. The mass spectra were calibrated using common hydro-

carbon fragment peaks at CH_3^+, $C_2H_3^+$, and $C_4H_7^+$. For the tissue reproducibility experiment, sections 1 through 10 were analyzed. Four tissue types were selected for analysis: brain, rib, heart and liver. Two to ten measurements were recorded for each tissue type depending on the sizes of the tissue regions available in each slice. Each of the ten samples was analyzed twice over a period of 1 month in order to monitor the reproducibility and stability of data. Spectra for background controls were acquired by analyzing clean silicon areas on the wafers. Contamination peaks were identified from the background control spectra and excluded in the later PCA analysis. Excluded peaks are attributable to primary ion source elements ($m/z = 69$, 133), polydimethylsulfoxide contamination ($m/z = 73$, 147, 207, 221, 281) and most likely deparaffinization and other sample preparation steps ($m/z = 71$, 74, 83, 91, 97, 115, 117, 119, 125, 148, 149, 169, 191, 219, 242, 279, 282, 283, 325, 399, 421, 459).

2.4. Principal component analysis

Principal component analysis (PCA) was used to analyze the spectra and images obtained from the measurements. Specifically, data reduction was accomplished using MATLAB v. 7.0 (MathWorks Inc., Natick, MA) along with PLS Toolbox v. 3.5 (Eigenvector Research, Manson, WA). Unit mass binning was applied to each spectrum with the exception of $m/z = 40$, which contained only the calcium (Ca) peak. Masses from $m/z = 60$ to 500 and $m/z = 40$ (Ca) were used for data analysis. Identified contamination peaks were excluded from the PCA data reduction as discussed above. The resulting spectral dataset was normalized to that spectrum's total ion counts and then mean-centered before PCA. A scores plot with ninety percent data contours and loading plot were then generated. Ninety percent data contours were drawn using the error_ellipse.m code by J. Andrew Johnson of Binghamton University, acquired from the MATLAB Central File Exchange.

3. Results and discussion

3.1. ToF-SIMS imaging of different tissue types

The optical image of a 16-day-old H&E stained mouse embryo section is shown in Fig. 1(a). Representative positive total ion ToF-SIMS images obtained from specific tissue areas of a comparable mouse embryo section are shown in Fig. 1(b)–(e). These ToF-SIMS images illustrate that there is sufficient chemical information left in the fixed tissues to produce ion images that highlight the tissue structure. The ion images allow comparisons among the different tissues with regards to molecular density and structural information.

Fig. 2 shows the positive ion images of tissue regions acquired from the rib and the heart. These images, which represent all of the ions desorbed from the surface of the sample, can also be presented to show the specific distribution of a particular mass of interest. The distribution of $m/z = 23$ (sodium, (Na)) in the rib is shown in Fig. 2(b). This Na image clearly shows the structure of the developing rib bone within the matrix of other soft tissues. Fig. 2(d) shows the distribution of $m/z = 70$ in the heart section. A high mass resolution spectrum acquired using bunched mode determined that this peak is C_4H_8N, which we have shown to be a fragment of the amino acids arginine and proline (data not

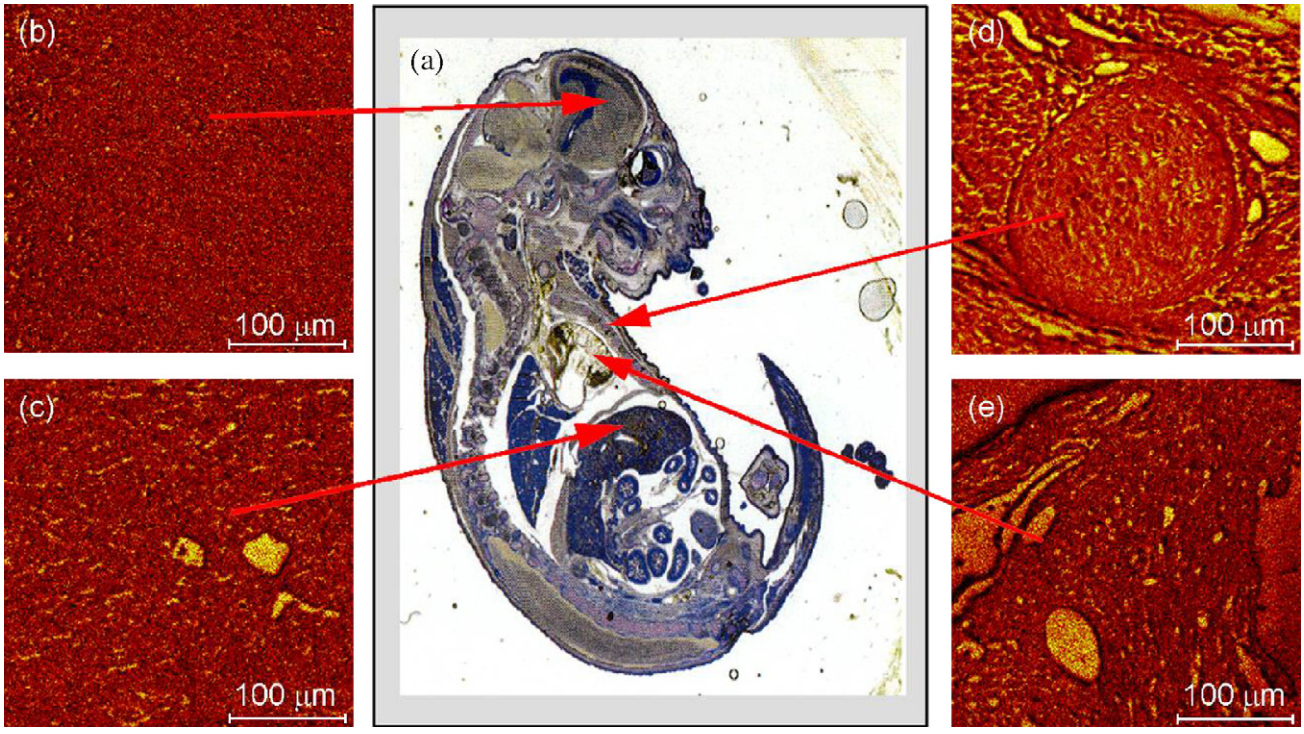

Fig. 1. (a) Optical image of a 16-day-old H&E stained mouse embryo section. (b) Positive total ion ToF-SIMS image of brain. (c) Positive total ion ToF-SIMS image of liver. (d) Positive total ion ToF-SIMS image of rib. (e) Positive total ion ToF-SIMS image of heart. Arrows point to the corresponding tissue region in the optical image.

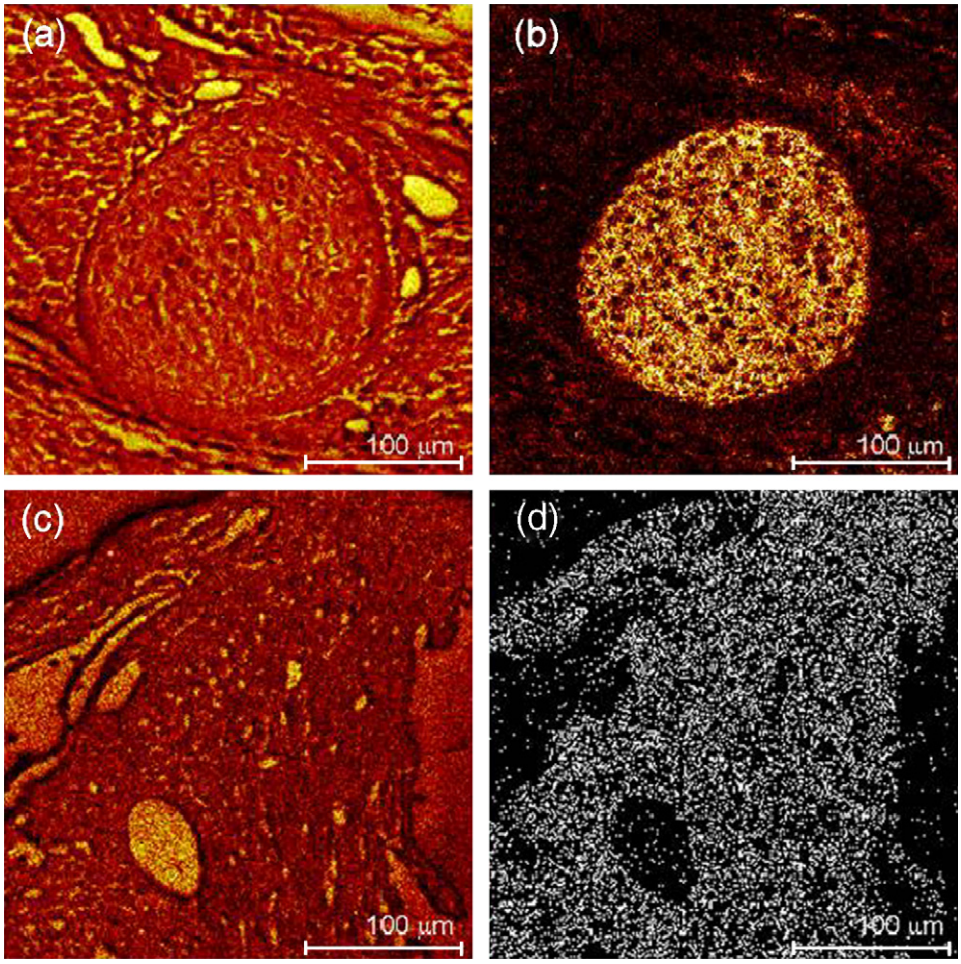

Fig. 2. (a) ToF-SIMS positive total ion image of a rib. (b) $m/z = 23$ (sodium) distribution of (a). (c) Positive total ion image of a region of the heart. (d) $m/z = 70$ (C_4H_8N) distribution of the region shown in (c).

shown). Univariate imaging analysis is helpful in defining the regions of interest (ROIs) of tissues and for visualizing the distribution of particular chemicals or molecular fragments. However, the spectra from different tissues are very similar and impossible to differentiate using univariate analysis. Multivariate analysis is needed for differentiating tissue types.

3.2. Differentiation of tissue types by PCA

To determine our ability to differentiate tissues using PCA, positive ion mass spectra from 6 different tissues of tissue section number 10 were acquired and analyzed. Ten regions from each brain, spinal cord, skull, rib, heart and liver were converted to spectra and used for the analysis. Low mass peaks (below $m/z = 60$, C_4 and smaller hydrocarbon clusters) were removed from the PCA calculation to exclude these hydrocarbon peaks that carry no specific chemical information. Background peaks were identified and also removed from the analysis, as described in the Experimental section. Fig. 3(a) shows the scores plot of the first principal component (PC1) and the second principal component (PC2) axes. Together, these two PCs capture approximately 95% of the variance among the data groups. Each point in the scores plot represents a mass spectrum acquired from one specific tissue area; spectra from different tissue types are denoted by different color symbols. The ellipses surrounding each group represent the 90% data contour for that group. This plot shows that the spectra from each tissue type are tightly clustered and that the tissues are separated according to chemical composition. The bone-derived skull and rib groups, which contain a higher mineral concentration, are well-separated from nervous tissue (brain and spinal cord) and the heart and liver. The corresponding PCA loading plot illustrated in Fig. 3(b) shows that $m/z = 40$ (calcium (Ca)) is the variable primarily responsible for differentiating the skull and rib from the less-mineralized tissues.

Further examination of the scores plot (Fig. 3(a)), shows that the brain and spinal cord groups exhibit considerable overlap, denoting the similar molecular composition of these two tissue types. Nervous tissue contains a high concentration of phospholipids, primarily from the myelin that surrounds the axons or nerve cells [33]. Although lipids are mostly lost during the tissue fixation process, the chemical information that remains in the molecular matrix that supports the phospholipids is sufficient to clearly differentiate these tissues from the heart and liver spectra. Heart tissue, which is primarily made up of cardiac muscle cells, and liver tissue, which is composed of hepatocytes, contains a higher concentration of cellular protein. These molecular

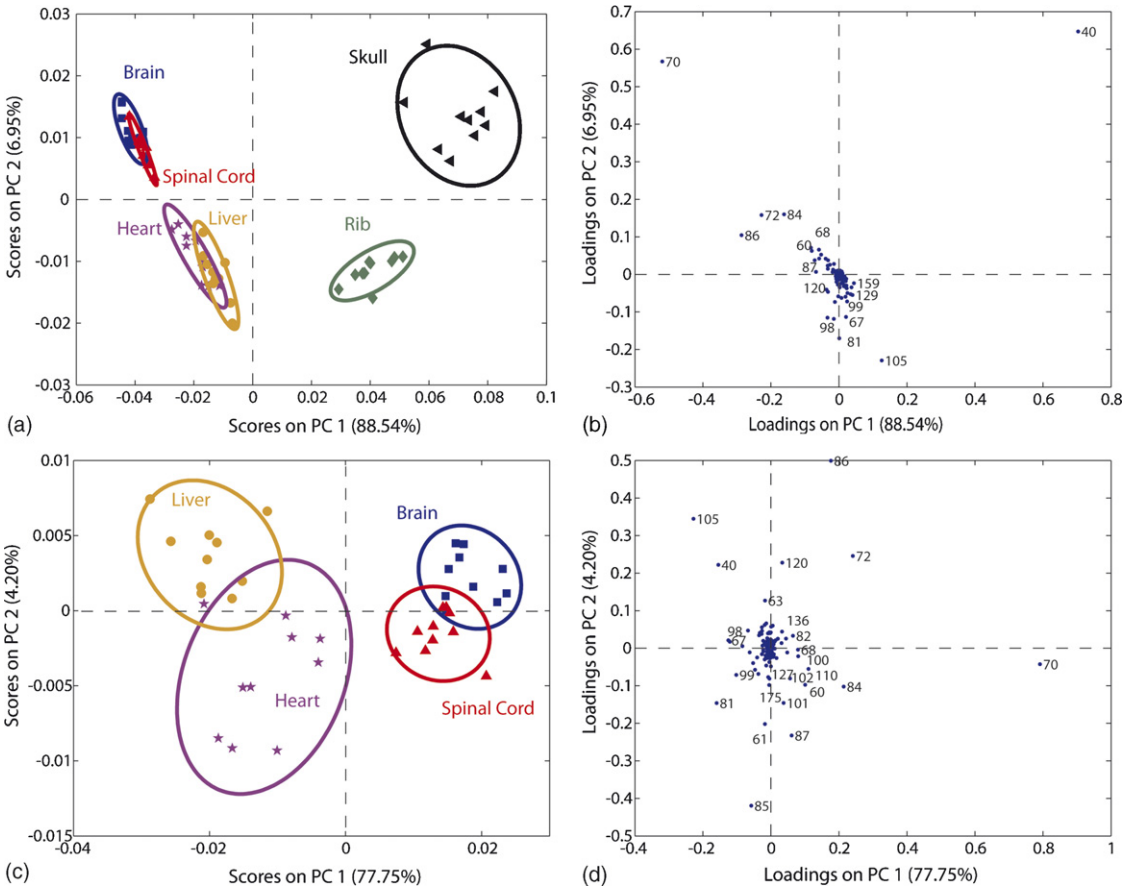

Fig. 3. (a) Scores plot of PC1 vs. PC2 of spectra from six tissues with 90% data contour of each tissue. (b) Loading plot of same tissues. (c) Scores plot of PC1 vs. PC2 of spectra from heart, liver, brain and spinal cord. (d) Loading plot of same tissues.

differences produce a different pattern of peaks in the ToF-SIMS spectra that can be differentiated by PCA. Thus, the results seen in the scores plot in Fig. 3 are confirmed by the known biology of the various tissues.

In an effort to extend our ability to separate the soft tissues, we removed the skull and rib spectra from the PCA calculation and repeated the statistical analysis. Fig. 3(c) and (d) show the resulting scores and loadings plots using only the spectra acquired from the brain, spinal cord, heart and liver tissues. Although the scores plot (Fig. 3(c)) shows a slight overlap in the 90% data contours of the brain/spinal cord and heart/liver groups, essentially the four soft tissues are well separated. The nervous tissues, brain and spinal cord, are separated from the heart and liver groups on PC1 and the heart and liver are separated on PC2. Given that the heart and liver are composed of different cell types and have different physiological functions, this is to be expected. More surprisingly, the brain and spinal cord are also separated on PC2. These two tissues, which are part of the central nervous system, are both composed essentially of neurons. The primary anatomical difference between the brain and the spinal cord is the arrangement of the grey and white matter [34]. In the spinal column the grey matter (the neuronal cell bodies) are on the inside and surrounded by white matter (axons, or the fibers that connect the neurons). In the brain's cerebral cortex, the grey matter surrounds the white matter. Depending on the exact location of the section through the embryo, it is possible that the spectra acquired from these two organs differed in the amount of white or grey matter being sampled. It is likely that the chemical composition of the white matter, which is covered by a dense layer of myelin, would be distinctly different from grey matter, which may account for the differences in the spectral patterns. Because the lipids that would be associated with the myelin in these tissues are lost during the fixation process, the differences in the spectral patterns could be a result of differing protein compositions in the grey and white matter. Examining the corresponding loadings plot (Fig. 3(d)) shows that peaks at $m/z = 70$, 72, 84, 86 and 120 are closely related to the brain and spinal cord (which can also be noted in Fig. 3(b)). Although the logical next step for this research is to assign the identity of the peaks that drive the differentiation of the tissues, conclusively determining the origin of these molecular species cannot be done at this time. We are currently pursuing studies to identify these fragments; these studies will allow us to understand the biological differences in the samples that give rise to the chemical differences that we see among the spectra.

3.3. Reproducibility and stability of the ToF-SIMS method

In order to understand both the reproducibility of the ToF-SIMS method, as well as the chemical stability of the samples,

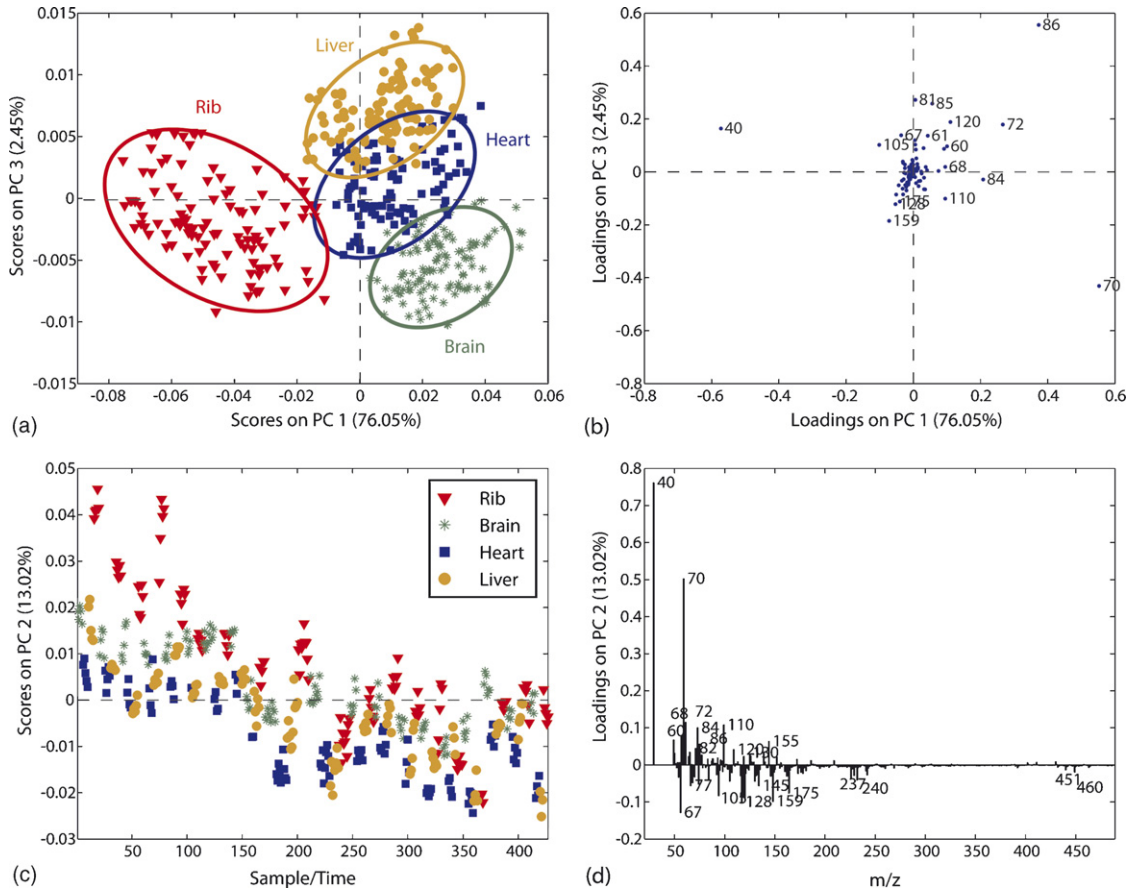

Fig. 4. (a) Scores plot PC1 vs. PC3 for four tissues (brain, heart, liver and rib) with 90% data contours drawn for each tissue. (b) Loading plot of PC1 vs. PC3 for the four tissues. (c) Scores plot of PC2 vs. sample number (time) for the same data depicted in (a). (d) Loading plot of PC2 for the same data.

we did repeated measurements of the embryos over the period of 1 month. These studies are necessary in order to identify potential sources of variation in that may occur during the analysis of paraffin-embedded clinical samples. Clinical samples are frequently stored under minimally controlled conditions for extended periods of time and may vary depending upon individual laboratory sample processing procedures. Understanding the reproducibility and stability of the method is essential for future applications of ToF-SIMS to paraffin-embedded samples.

To determine the stability and reproducibility of the experiment, spectra from four tissue types: rib, brain, heart and liver of ten embryo sections, were acquired twice over a period spanning 1 month. This entire spectral data set (including the corresponding spectra of the differentiating experiment above), composed of 427 spectra, was then analyzed by PCA. Fig. 4(a) and (b) shows the scores and loading plots of the first principal component (PC1) and third principal component (PC3) axes. The scores plot, Fig. 4(a), shows a good separation of the four tissue types. The variation within the sample dataset is mainly from three sources: (1) inherent biological variation within the samples, (2) environmental contamination of the sections and (3) changes in the sample during storage. Biological variation is to be expected in these samples; the spectra acquired from the tissues were taken from three embryos that were obtained from three different dams. Although using the same strain of mice for the experiment assures a consistent genetic background among the mice, phenotypic variation among individuals contributes to the sample variation. The second source of variation, environmental contamination, is most frequently demonstrated as differences in the amount of PDMS among the embryos. In this experiment, there was a higher concentration of PDMS in embryos 2 and 3 (sections 4–9). The PDMS appears to have been introduced into the sample before sectioning and deparaffinization because all of the samples were handled and processed at the same time, under identical conditions. Although the majority of the sample scattering due to PDMS can be removed from the analysis by removal of PDMS-related peaks ($m/z = 73$, 147, 207, 221, 281), differences in the samples due to the matrix effect of PDMS cannot be removed or accounted for and results in variations among the samples.

The third source of variation is change in the samples during storage. In Fig. 4(c) the scores on PC2 are plotted as a function of sample number. In these data increasing sample number is also related to storage time; higher sample numbers correspond to spectra that had been acquired from samples that had been stored longer. We believe that changes seen in the samples along PC2 demonstrate chemical changes in the samples due to storage. The corresponding plot, Fig. 4(d), indicates that over time the samples have a relatively decreased signal intensity for the even number peaks (peaks that commonly represent

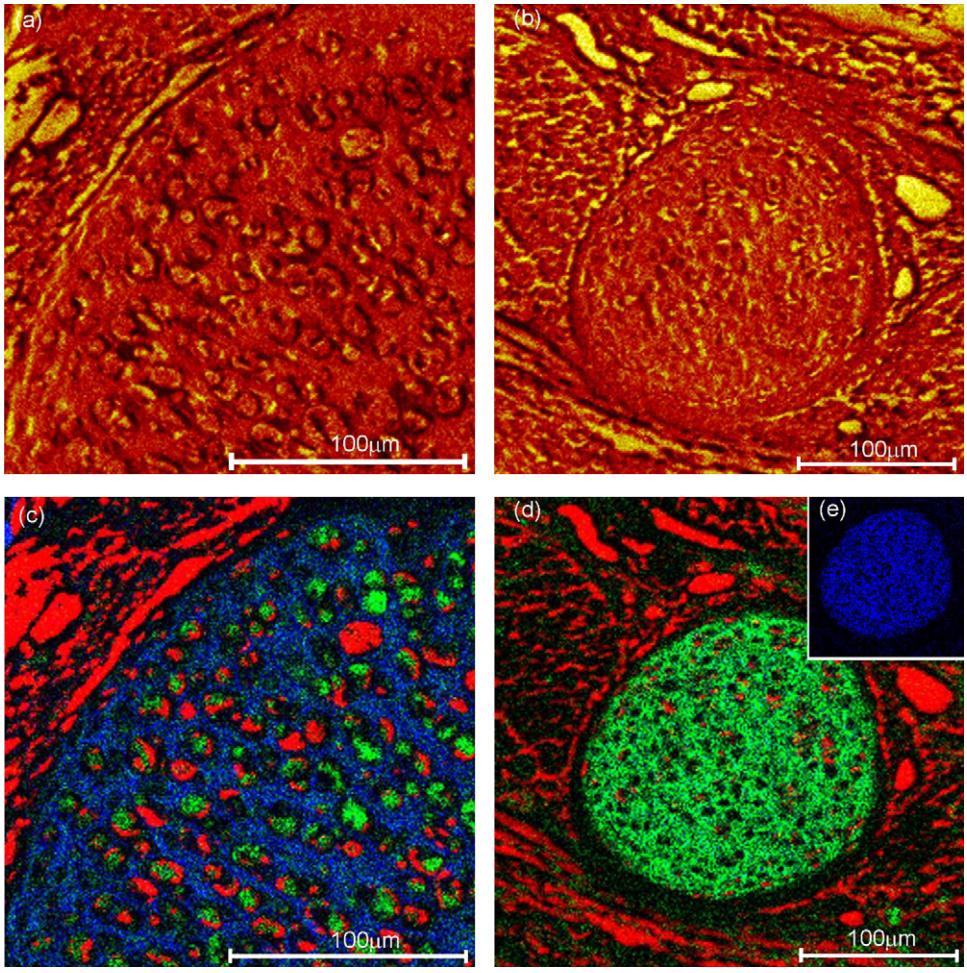

Fig. 5. (a) ToF-SIMS positive total ion image of a region of the skull. (b) ToF-SIMS positive total ion image of a rib. (c) Three-color overlay of the skull image; red color represents the Si substrate; green color represents the Na distribution; blue color represents the Ca distribution. Na and Ca are plotted on the same scale: (d) three-color overlay of the rib image, red color represents the Si substrate; green color represents the Na; blue color (too low to be visible) represents the Ca distribution. Na and Ca are plotted on the same scale: (e) Ca distribution with the signal intensity increased 5×.

organic materials) and an increased signal intensity for the odd number peaks (hydrocarbon peaks). Since samples were stored under vacuum, volatile organic compounds could be gradually depleted over time, causing the relative decrease in the even numbered peaks. Comparing background spectra from just the silicon areas of the sample wafers, taken at different times, indicates that there was an increasing intensity of peaks attributed to PDMS as well as some unknown peaks at $m/z = 647$ and 662. These contaminating peaks could have been introduced when the vacuum was released and samples were exposed to air, or they could be contamination from the vacuum system itself, i.e., pump oil. Even through PDMS and other identified contamination peaks are removed from the PCA calculation, the matrix effects from those peaks may also affect the calculation results. These results demonstrate the need for a well-controlled sample storage protocol for future studies.

3.4. Differentiating the development of bone with time

ToF-SIMS positive total ion images obtained from sections of skull and rib are shown in Fig. 5(a) and (b), respectively. These images clearly demonstrate structural details and molecular variation between these two types of bones. Detailed analysis of the images was conducted by displaying three of the major chemical components of the samples in the color overlay images illustrated in Fig. 5(c) and (d). The distribution of the background silicon ions ($m/z = 28$) is colored red, the distribution of the Na ions ($m/z = 23$) is colored green and the distribution of the Ca ions ($m/z = 40$) is colored blue. To provide direct visual comparison, the Na and Ca signal intensities were set to the same scale in each overlay image.

Comparing the overlay images of the skull (Fig. 5(c)) and the rib (Fig. 5(d)) shows that calcium is the most abundant element in the skull whereas sodium dominates in the rib. The insert in Fig. 5(d) (Fig. 5(e)) shows an image of the calcium distribution with the signal enhanced (5× brighter than Fig. 5(d)). This image illustrates that the calcium and sodium distributions are co-localized, without significant spatial separation. A further quantitative analysis can be done by calculating a ratio of the calcium to sodium signal intensity for both images. The counts ratio of Ca/Na is 1.425 for skull and 0.209 for the rib, confirming the higher concentration of Ca in the skull. The differing

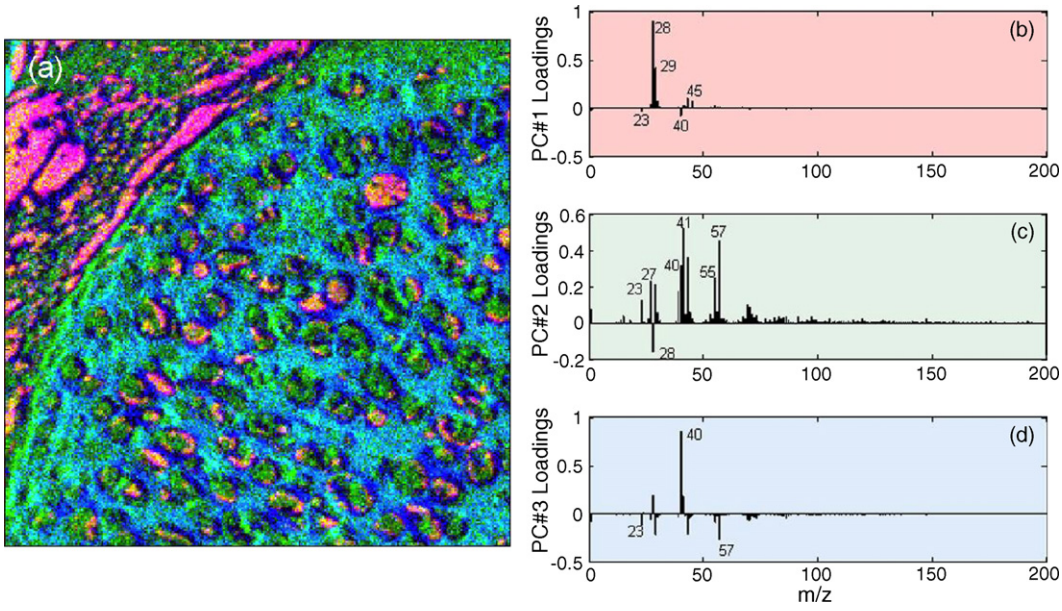

Fig. 6. (a) Scores plot PC1, PC2 and PC3 overlay of skull image. Red color is PC1; green color is PC2; blue color is PC3. (b) Loading plot of PC1. (c) Loading plot of PC2. (d) Loading plot of PC3.

developmental paths known to occur in these two types of bone confirm this observation. The flat bones of the skull develop by intramembranous ossification and in an embryo 16 days old these fetal bones have begun to ossify and concentrate calcium [32]. In contrast, rib bones develop by endrochondral ossification, a process of mineralizing hyaline cartilage into hardened bone. The rib bones of the embryos under examination are still primarily cartilage [32], which consists mainly of a matrix of collagen and proteoglycans [35]. The negative charges of the sulfate and carboxylate groups within the proteoglycans attract a high concentration of Na ions to maintain overall electroneutrality. In normal cartilage the Na concentration is proportional to the proteoglycan concentration [36]. Therefore the high concentration of Na in the rib image is a result of the cartilaginous nature of this developing bone.

3.5. Image PCA analysis of skull

As shown in Figs. 1–5, the most common method for interpreting ToF-SIMS images relies on univariate analysis to display selected individual variables or peaks. In practice, due primarily to the quantity of data, it can be difficult to identity important signals in the data using just univariate analysis methods. Furthermore, establishing correlations among relevant masses in a complex spectral image setting is often arduous. For instance, because different parent compounds produce similar molecular fragments, specific organic species can be difficult to resolve in ToF-SIMS images. Poor chemical contrast in the images is a direct consequence.

One approach to solving this difficulty is to apply multivariate analysis to the entire spectral image dataset. This reduces the large spectral image dataset to a physically realizable form that highlights the relevant chemical components of the image. Such an approach is in essence conducting statistical analysis directly on a large number of sequentially labeled mass spectra, which are embedded in the image. The result of the calculation is displayed as a false-colored image with each color representing a group of correlated molecular information.

Fig. 6(a) shows the result of image-PCA analysis of the ion image of the region of the skull previously shown in Fig. 5. In image-PCA the colors represent the PCs and thus are correlated to molecular information specific to each principal component. In this analysis, the first three PCs are represented by three colors: red (PC1), green (PC2) and blue (PC3). The plot Fig. 6(b) shows the corresponding mass peaks that contain the variation in the dataset and drive the separation. In this image, the red area is correlated with the silicon substrate ($m/z = 28$), SiH ($m/z = 29$) and SiOH ($m/z = 45$); the green area is correlated with Na ($m/z = 23$) and hydrocarbon peaks ($m/z = 27$, 41, 43, 55, 57 and so on); and the blue color is mainly correlated with Ca ($m/z = 40$). The distribution of Ca shows the structure of the developing bone. The green areas, which represent the soft tissues within the bone structure, are anti-correlated to silicon. This statistically derived false color image shows both the correlation and anti-correlation of important mass peaks within a certain area. In our example, the PCA image (Fig. 6(a)) is comparable to the overlay image (Fig. 5(a)). However, the PCA image was created without *a priori* knowledge of the important mass peaks that show the differences in the image. In more complicated analyses, where the identity of the most variable masses is truly unknown, image-PCA would be able to highlight differences within the image that are not apparent on visual inspection. For FFPE tissues, application of this method could be used to identify changing regions within the tissues that are indicative of disease. Further analysis of the diseased regions by imaging PCA could be used to improve tissue-based diagnosis, predict response to specific modes of treatment, and aid pathologist in their prognosis decisions.

4. Conclusions

Even with processed tissues that were paraffin-embedded and then deparaffinized, ToF-SIMS and PCA can separate different tissue types from mouse embryos. Studies of the reproducibility of the method show that the separation of tissues is reproducible across three different embryos and over the span of 1 month. Further studies need to be done to determine the best way to control sample contamination and ideal storage conditions to minimize the sample variation. This work shows that ToF-SIMS and image-PCA can be used to identify changes in the structure of highly processed tissues. The application of this method in future studies could be to identify changing regions within the tissues that are indicative of disease. Further analysis of the diseased regions could be used to improve tissue-based diagnosis, predict response to specific modes of treatment, and aid in prognosis decisions.

Acknowledgments

This work was performed under the auspices of the U.S. Department of Energy by the University of California, Lawrence Livermore National Laboratory under contract no. W-7405-Eng-48. Additional support from National Cancer Institute grant CA55861, CA BCRP 10IB-0077 and LDRD 04-ERD-104 and 06-FS-007 is gratefully acknowledged.

References

[1] M. Jaremko, C. Justenhoven, B.K. Abraham, W. Schroth, P. Fritz, S. Brod, C. Vollmert, T. Illig, H. Brauch, Hum. Mutat. 25 (2005) 232.
[2] S. Chandra, J. Microsc.-Oxford 204 (2001) 150.
[3] S. Chandra, D.R. Lorey, D.R. Smith, Radiat. Res. 157 (2002) 700.
[4] I.M. Kempson, W.M. Skinner, P.K. Kirkbride, Biochim. Biophys. Acta 1624 (2003) 1.
[5] T.P. Roddy, J.D.M. Cannon, S.G. Ostrowski, N. Winograd, A.G. Ewing, Anal. Chem. 74 (2002) 4020.
[6] D.M. Cannon, M.L. Pacholski, N. Winograd, A.G. Ewing, J. Am. Chem. Soc. 122 (2000) 603.
[7] B. Cliff, N. Lockyer, H. Jungnickel, G. Stephens, J.C. Vickerman, Rapid Commun. Mass Spectrom. 17 (2003) 2163.
[8] B. Cliff, N.P. Lockyer, C. Corlett, J.C. Vickerman, Appl. Surf. Sci. 203/204 (2003) 730.
[9] P. Sjovall, J. Lausmaa, B. Johansson, Anal. Chem. 76 (2004) 4271.
[10] S.G. Ostrowski, C.T. Van Bell, N. Winograd, A.G. Ewing, Science 305 (2004) 71.
[11] E. Gazi, J. Dwyer, N. Lockyer, P. Gardner, J.C. Vickerman, J. Miyan, C.A. Hart, M. Brown, J.H. Shanks, N. Clarke, Faraday Discuss. 126 (2004) 41, discussion 77–92.
[12] J.N. Quong, M.G. Knize, K.S. Kulp, K.J. Wu, Appl. Surf. Sci. 231/232 (2004) 424.
[13] A.M. Belu, D.J. Graham, D.G. Castner, Biomaterials 24 (2003) 3635.
[14] P.J. Todd, T.G. Schaaff, P. Chaurand, R.M. Caprioli, J. Mass Spectrom. 36 (2001) 355.
[15] D. Touboul, F. Halgand, A. Brunelle, R. Kersting, E. Tallarek, B. Hagenhoff, O. Laprevote, Anal. Chem. 76 (2004) 1550.
[16] K. Borner, H. Nygren, B. Hagenhoff, P. Malmberg, E. Tallarek, J.E. Mansson, Biochim. Biophys. Acta 1761 (2006) 335.
[17] H. Nygren, C. Eriksson, P. Malmberg, H. Sahlin, C. Lennart, J. Kausmaa, P. Sjovall, Colloids Surf. 30 (2003) 87.
[18] H. Nygren, K. Borner, B. Hagenhoff, P. Malmberg, J.E. Mansson, Biochim. Biophys. Acta 1737 (2005) 102.
[19] N.P. Lockyer, J.C. Vickerman, Appl. Surf. Sci. 231/232 (2004) 377.
[20] M. Fartmann, C. Kriegeskotte, S. Dambach, A. Wittig, W. Sauerwein, H. Arlinghaus, Appl. Surf. Sci. 231/232 (2004) 428.
[21] K.S. Kulp, E.S.F. Berman, M.G. Knize, D.L. Shattuck, E.J. Nelson, L. Wu, J.L. Montgomery, J.S. Felton, K.J. Wu, Anal. Chem. 78 (2006) 3651–3658.
[22] M.S. Wagner, D.G. Castner, Appl. Surf. Sci. 231/232 (2004) 366.
[23] S. Pachuta, Appl. Surf. Sci. 231/232 (2004) 217.
[24] M.S. Wagner, B.J. Tyler, D.G. Castner, Anal. Chem. 74 (2002) 1824.
[25] C.E. Thompson, H. Jungnickel, N.P. Lockyer, G.M. Stephens, J.C. Vickerman, Appl. Surf. Sci. 231/232 (2004) 420.
[26] M.E. Kargacin, B.R. Kowalski, Anal. Chem. 58 (1986) 2300.
[27] M.S. Wagner, D.G. Castner, Langmuir 17 (2001) 4649.
[28] M.S. Wagner, M. Shen, T.A. Horbett, D.G. Castner, J. Biomed. Mater. Res. 64A (2003) 1.
[29] M.S. Wagner, D.J. Graham, B.D. Ratner, D.G. Castner, Surf. Sci. 570 (2004) 78.
[30] H. Jungnickel, E.A. Jones, N.P. Lockyer, S.G. Oliver, G.M. Stephens, J.C. Vickerman, Anal. Chem. 77 (2005) 1740.
[31] R.I. Freshney, Culture of Animal Cells, A Manual of Basic Technique, John Wiley and Sons, New York, 2000.
[32] K. Theiler, The House Mouse: An Atlas of Embryonic Development, Springer-Verlag, New York, 1989.
[33] M. Spohn, A.N. Davison, J. Lipid Res. 13 (1972) 563.
[34] J.H. Martin, Neuroanatomy: Text and Atlas, McGraw-Hill, New York, 2003.
[35] A. Maroudas, Physicochemcial Properties of Articular Cartilage, Pitman Medical, Kent, England, 1979.
[36] S.L. Carney, H. Muir, Physiol. Rev. 68 (1988) 858.